Naturally Derived Allylated Gallic Acid for Interfacially Polymerized Membranes

ACS Sustainable Chemistry & Engineering

pubs.acs.org/journal/ascecg

Research Article

Naturally Derived Allylated Gallic Acid for Interfacially Polymerized Membranes

Banan Alhazmi, Fadhilah Alduraiei, Priyanka Manchanda, Stefan Chisca, Gyorgy Szekely, and Suzana P. Nunes*

Cite This: https://doi.org/10.1021/acssuschemeng.2c02637

Read Online

ACCESS | Metrics & More | Article Recommendations | Supporting Information

ABSTRACT: A naturally derived monomer, allylated gallic acid (AG), was herein proposed as a monomer for interfacially polymerized thin-film composite nanofiltration membranes. We investigated the synthesis of the thin-film composite polyester membranes by varying the concentration of the AG monomer and the reaction time with trimesoyl chloride. In addition, we demonstrated the synthesis of a polyesteramide film using a mixture of AG and *m*-phenylene diamine, although there are a few orders of magnitude differences in their reactivity. While membranes prepared using the classical polyamide process had a water permeance of 0.54 L m^{-2} h^{-1} bar^{-1} , the prepared polyesteramide and polyester films had water permeances of 12.3 and 47.6 L m^{-2} h^{-1} bar^{-1}, respectively The rejection of dyes was larger than 700 g mol^{-1} and could be tuned to 327 g mol^{-1} by changing the chemical composition and reaction time. The retention of inorganic salts followed the order Na_2SO_4 > $MgSO_4$ ≈ NaCl. Therefore, the membrane performance demonstrates the potential of the phenolic monomer to be integrated into the synthesis of thin-film composite membranes. Besides, the availability of the free allyl group holds potential for further modification and covalent binding onto the surface.

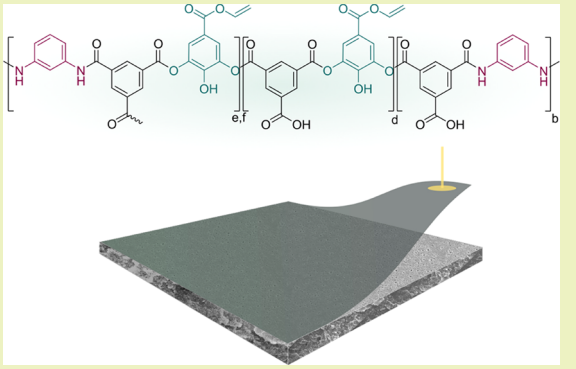

KEYWORDS: *green chemistry, natural precursor, interfacial polymerization, nanofiltration, thin film*

1. INTRODUCTION

Water is massively used in the textile industry, producing thereof an equal amount of textile wastewaters that contain organic dyes and inorganic salts. For instance, Congo red (CR), a synthetic anionic diazo dye, is often employed as a pigment in the textile industry and can degrade to carcinogenic compounds that pose a major threat to the environment and public health if left untreated.[1,2] Conventional methods like coagulation, flocculation, and adsorption have a great potential for the removal of dyes from industrial wastewaters, but the chemicals involved and the resulting solid waste can be another source of pollution.[3,4] Alternatively, nanofiltration is an attractive pressure-driven membrane-based technology. Nanofiltration is effective for the separation of solutes with molecular weights in the range of 200−2000 g mol^{-1}, operating between ultrafiltration and reverse osmosis.[5,6] Therefore, it has been integrated in various applications for water purification and wastewater treatment.[7]

An important class of nanofiltration membranes is thin-film composite (TFC) membranes, which consist of a thin selective barrier that can be tailored to address the needs of each separation. High-performance TFC membranes are effectively prepared on an industrial scale by interfacial polymerization.[5] Cadotte[8] was the first to introduce reverse osmosis membranes fabricated using this method. His original procedure involved the formation of a hyper-cross-linked aromatic polyamide film using *m*-phenylene diamine (MPD) or piperazine (PIP) dissolved in water and trimesoyl chloride (TMC) in hexane. The resulting TFC membranes have been responsible for the success of large-scale seawater desalination in many countries.[9,10] TFC membranes for seawater desalination are relatively hydrophilic and have been developed to fully reject salts and allow water transport. However, by choosing other monomer combinations and the right porous substrates, the selectivity of the membranes can be fine-tuned for challenging separations of small molecules by size, charge, and form. Developments on membranes prepared by interfacial polymerization have been a topic of excellent recent reviews.[11−13]

Typical nanofiltration TFC membranes show excellent retention of small organic molecules and multivalent ions. However, such membranes suffered when treating textile

Received: May 7, 2022
Revised: August 4, 2022

wastewater that contains organic dyes and ionorganic salts. The high osmotic pressure can cause a decline in the water flux when the concentration of ions in feed solution increases, which can limit the efficiency of fractionating organics from wastewaters.[14] In that sense, fine-tuning the structure of the selective films to retain high water flux and superior rejection of organics have attracted great attention for the removal of dyes from industrial waste streams.[15−17] Composite membranes prepared using different piperazine-based derivatives, for example, demonstrated the influence of the diamine structure on the surface charge, morphology, and performance of the membrane.[18] These membranes exhibited different rejection rates of mono- and multivalent ions with water permeance in the range 8.8−3.1 L m^{-2} h^{-1} bar^{-1}.

Natural or bioinspired monomers are emerging as an alternative to the classical amines and acid chlorides. Inspired by mussel adhesive proteins, Lee et al.[19] were the first to use dopamine self-polymerization to form thin films on a diverse array of substrates. A few studies also investigated the use of dopamine and acid chloride as precursors for interfacial polymerization.[20−22] Because of their structural similarities to dopamine, low-cost, and rather additional versatility, a collection of plant-derived phenols has also been attractive for polymeric membrane synthesis and modification.[23−30] Figure S1 shows a number of selected phenol structures that could be used for polymerization.[31−35] Tannic acid, particularly, has been reported as a building block for interfacial polymerization. In a pioneer study conducted by Zhang et al.,[31] the aqueous nanofiltration performance of the TFC membranes fabricated using tannic acid revealed a water permeance between 13 and 50 L m^{-2} h^{-1} bar^{-1} with Orange GII rejection well above 98% for all reaction times above 5 min and approximately 50% retention of Na_2SO_4. In a recent study, this high retention of dyes was obtained at high salts permeation when tannic acid and piperazine were combined into a longer monomer to achieve a loose active layer. This membrane exhibited a water permeance of 33 L m^{-2} h^{-1} bar^{-1} and salts rejections of 9.4 and 12.3% for, respectively, Na_2SO_4 and $MgSO_4$.[32]

In line with the reported studies, a novel natural phenol, allylated gallic acid (AG), was herein introduced as a building block for interfacial polymerization. Besides being a naturally occurring triphenolic compound, the allyl groups could be potentially attractive for different postfunctionalizations and covalent binding onto the surface. The phenolic monomer was employed in the polar phase of the interfacial polymerization reaction with TMC in the organic phase. We investigated the effect of the monomer concentration and the reaction time on the synthesis of the selective film. We also studied the effect of the introduction of MPD to the polar phase of the reaction on the surface chemistry and morphology of the film. The nanofiltration performance of the fabricated TFC membranes exhibited excellent rejection of dyes greater than 700 g mol^{-1} and can be tuned up to 327 g mol^{-1}. A reasonable permeation of inorganic salts was observed, indicating the possibility of integrating the membrane for textile wastewater treatment.

2. MATERIALS AND METHODS

2.1. Materials. Polyacrylonitrile (PAN) porous membranes were supplied by GMT GmbH, Rheinfelden, Germany. Allyl 3,4,5-trihydroxybenzoate (allylated gallic acid, AG) (210.18 g mol^{-1}) was purchased from Specific Polymers. Trimesoyl chloride (TMC) (265.5 g mol^{-1}), *m*-phenylenediamine (MPD) (108.1 g mol^{-1}), sodium hydroxide (NaOH) (40 g mol^{-1}), methyl orange (MO) (327 g mol^{-1}), congo red (CR) (697 g mol^{-1}), direct yellow (DY) (957 g mol^{-1}), reactive green (RG) (1419 g mol^{-1}), linear polyethylene glycol (PEG), and trimethylol propane ethoxylate were all purchased from Sigma Aldrich. Sodium sulfate (Na_2SO_4), magnesium sulfate ($MgSO_4$), and sodium chloride (NaCl) were purchased from Fisher Scientific. Phosphate buffered saline (10× solution) and Isopar G were supplied by Fisher Scientific and Univar, respectively. Deionized water used in all experiments was filtered through a Millipore Milli-Q water purification system. All chemicals were used as received.

2.2. Membrane Fabrication. TFC membranes were fabricated by interfacial polymerization reaction between AG and/or MPD dissolved in phosphate buffer saline (pH 8.0) and TMC in Isopar G on top of PAN porous membranes. The pristine supports were mounted on a Teflon frame and impregnated with 10 mL of aqueous phase solution for 15 min. After removing the excess solution with air flow, the membranes' surface was exposed to 10 mL of the TMC solution. Finally, the membranes were washed with hexane three times to remove unreacted monomers, allowed to dry overnight, and stored in water until tested. The support impregnation and interfacial polymerization reaction were carried at room temperature. All other fabrication conditions are specified in Table 1. Freestanding films were prepared by adding 10 mL of aqueous and organic phase solutions into a glass Petri dish. The layers were collected from the interface and dried overnight at 60 °C under high vacuum for chemical analysis.

Table 1. Fabrication Conditions of TFC Membranes Prepared by Interfacial Reaction on PAN Support

abbreviation	AG [wt %]	MPD [wt %]	TMC [wt %]	$t_{reaction}$ [min]
TFC-$AG_{0.5}$-t_{180}	0.5	0	0.1	180
TFC-$AG_{0.5}$-t_{120}	0.5	0	0.1	120
TFC-$AG_{0.5}$-t_{90}	0.5	0	0.1	90
TFC-$AG_{0.5}$-t_{60}	0.5	0	0.1	60
TFC-$AG_{0.5}$-t_{20}	0.5	0	0.1	20
TFC-$AG_{1.0}$-t_{20}	1.0	0	0.1	20
TFC-$AG_{1.0}$-$MPD_{0.1}$-t_{20}	1.0	0.1	0.1	20
TFC-$AG_{1.0}$-$MPD_{0.3}$-t_{10}	1.0	0.3	0.1	10
TFC-$MPD_{0.1}$-t_{20}	0	0.1	0.1	20

2.3. Membrane Characterization. Attenuated total reflection-Fourier transform infrared (ATR-FTIR) spectra of the membranes were obtained using a Nicolet iS10 spectrometer. The measurements were carried out with 64 scans and a resolution of 4 cm^{-1}. The samples were washed rigorously with water and dried at 120 °C under high vacuum overnight. Solid-state ^{13}C nuclear magnetic resonance (NMR) experiments were recorded on a Bruker AVANCE III spectrometer operating at 400 MHz resonance frequency. X-ray photoelectron spectroscopy (XPS) experiments were performed on a Kratos Axis SUPRA instrument equipped with a monochromatic Al Kα X-ray source ($h\nu$ = 1486.6 eV) operated at 45 W under UHV conditions (approx. 10^{-9} mbar). The spectra were recorded in a hybrid mode using electrostatic and magnetic lenses and an aperture slot of 300 by 700 μm. The survey and high-resolution spectra were acquired at fixed analyzer pass energies of 80 and 20 eV, respectively. The samples were mounted in a floating mode to avoid differential charging, and thus, the spectra were acquired under charge neutralization conditions. The binding energy data were calibrated with respect to the C 1s signal at 284.5 eV. Prior to testing, the samples were washed rigorously with water and dried at 120 °C under high vacuum overnight.

Scanning electron microscopy (SEM) images were acquired on Nova Nano field-emission scanning electron microscope with an accelerating voltage of 5 kV and a working distance of 5 mm. The membranes were cut and mounted on an aluminum stub using a conductive aluminum tape. The cross-section samples were fractured in liquid nitrogen. To avoid surface charging, a 3 nm thick coating of

https://doi.org/10.1021/acssuschemeng.2c02637
ACS Sustainable Chem. Eng. XXXX, XXX, XXX−XXX

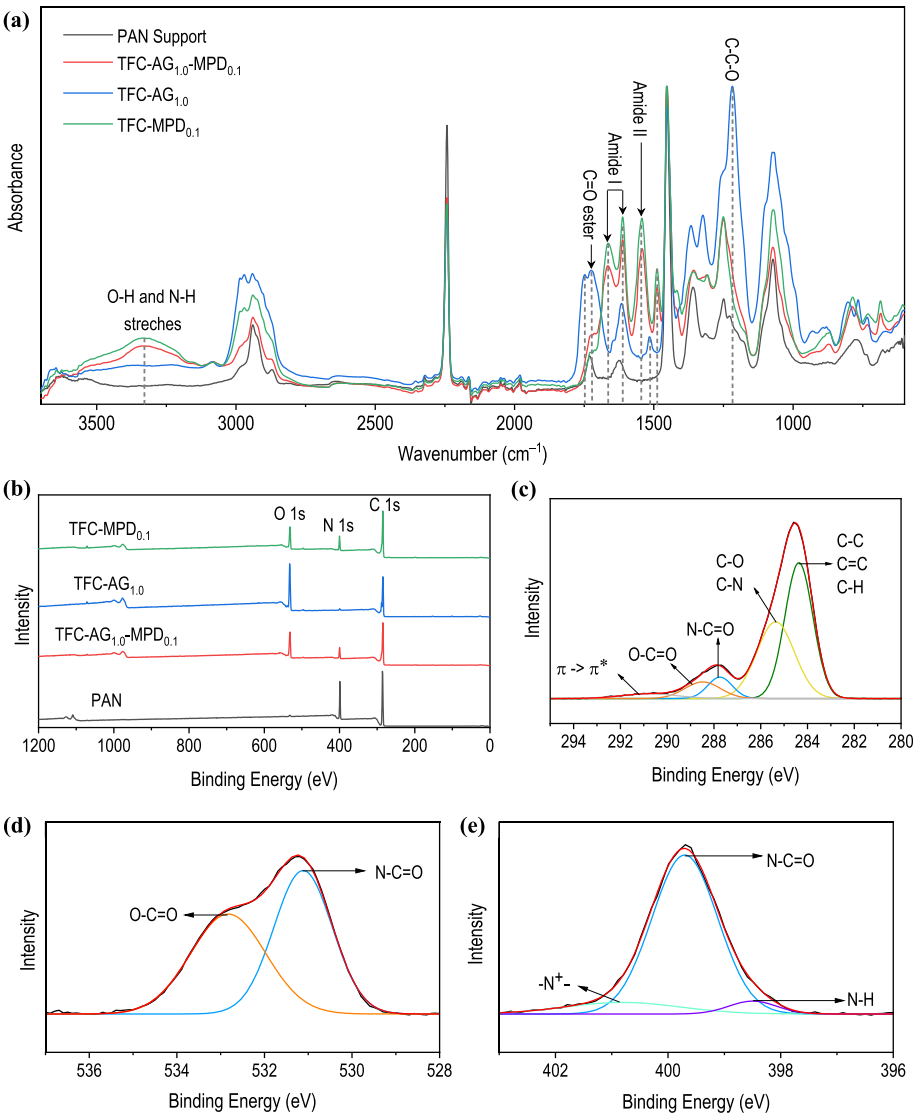

Figure 1. Chemical characterization. (a) FTIR spectra and (b) XPS survey spectra of the PAN porous support (in black) and TFC membranes prepared using 1 wt % AG/0.1 wt % MPD (in red), 1 wt % AG (in blue), and 0.1 wt % MPD (in green) as polar phase solutions. Deconvolution of (c) C 1s, (d) N 1s, and (e) O 1s high-resolution spectra for TFC-$AG_{1.0}$-$MPD_{0.1}$.

iridium was sputter-coated using Quorum Technologies Q150T under an argon atmosphere. Atomic force microscopy (AFM) images were obtained on a Dimension ICON scanning probe microscope under tapping mode in air to analyze the 3D morphologies and roughness of the membranes. The root mean square roughness (R_{ms}) was calculated for the height profile of each 5 μm × 5 μm.

To study the surface wetting nature of the membranes, water contact angles were evaluated via the sessile drop method using a goniometer on OCA 15EC, Dataphysics Instruments, at room temperature. A water droplet of 3 μL was carefully placed on the membrane using a microsyringe. The reported contact angle values are the averages of three measurements. The surface ζ potential was recorded for the thin-film composite membranes in aqueous solution at neutral pH using Zetasizer Nano series HT.

2.4. Membrane Performance. Aqueous nanofiltration experiments were carried at 5−20 bars using a dead-end stainless-steel cell at room temperature and under constant stirring of 400 rpm. The effective membrane area was 1 cm^2. Pure water, 10-20 ppm dye aqueous solution (RG, DY, CR, or MO), or 2000 ppm salt solution (Na_2SO_4, $MgSO_4$, or NaCl) were employed as feed to evaluate the filtration performance of the membranes. Table S1 shows the chemical structures and molecular weights of the dyes. Three parallel tests were performed to confirm the results. The permeance of water was measured for two hours and determined using eq 1:

$$P = \frac{V}{A \cdot t \cdot \Delta P} \tag{1}$$

where V = the permeate volume (L), A = the effective membrane area (cm^2), t = the filtration time (h), and ΔP = the applied pressure gradient (bar).

The solute rejection was determined using eq 2, where the feed (C_F), permeate (C_P), and retentate (C_R) concentrations were estimated from the ultraviolet−visible absorption spectrum recorded on a NanoDrop UV−vis spectrophotometer for dye solutions, while those of the salts were measured using a Eutech Instruments CON2700 conductivity meter. For each measurement, 200 mL of the solution was used as feed, the first 5 mL was discarded, and 3 samples of 5 mL were collected.

$$R\ (\%) = 100 \times \left(1 - \frac{C_P}{C_F}\right) \tag{2}$$

The rejection of PEGs with different molecular weights (0.6, 1, 3, and 35 kg mol^{-1}) was used to determine the molecular-weight cutoff (MWCO) for the membrane, which can be expressed by the

https://doi.org/10.1021/acssuschemeng.2c02637
ACS Sustainable Chem. Eng. XXXX, XXX, XXX−XXX

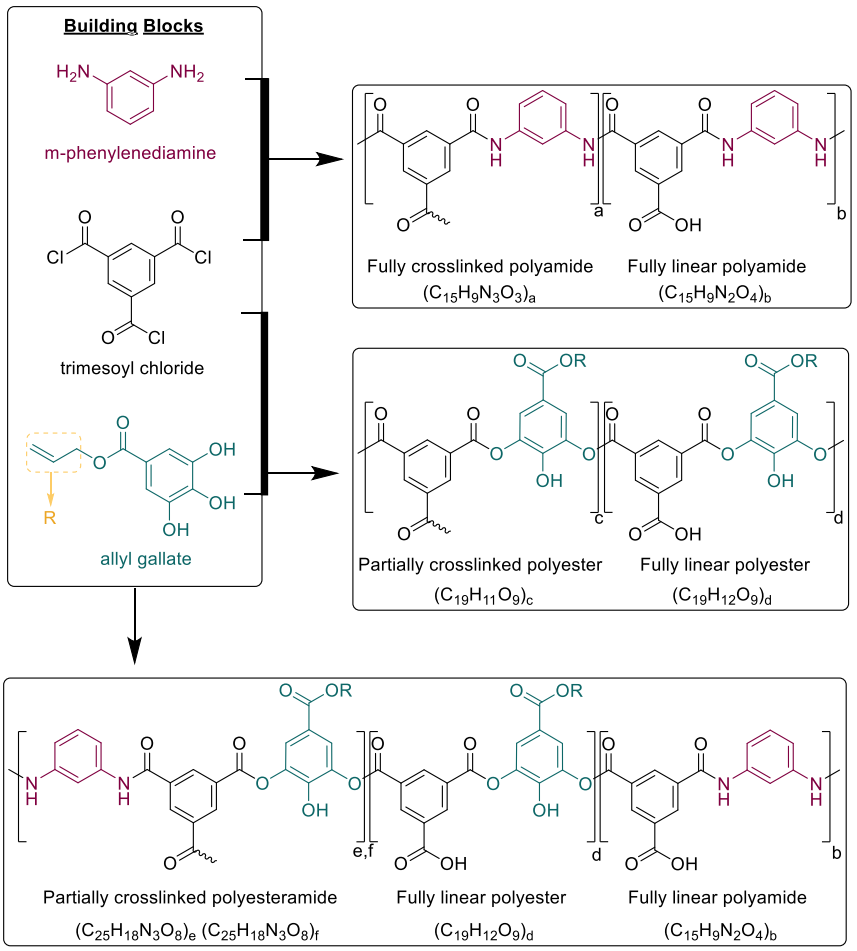

Figure 2. Basic interfacial polymerization reaction patterns of polyesteramide based on *m*-phenylene diamine (MPD), trimesoyl chloride (TMC), and allyl gallate (AG).

molecular weight corresponding to a reference compound that is typically rejected for 90%. The rejection value was determined using eq 2. The concentrations of the feed, permeate, and retentate sides were estimated from gel permeation chromatography recorded on an Agilent 1200 series system using deionized water as the effluent.

The long-term permeance and rejection tests using 20 ppm Congo red as feed were measured for one week.

3. RESULTS AND DISCUSSION

3.1. Membrane Chemical Characterization. The formation of polyester, polyesteramide, and polyamide films on top of a porous PAN support was initially investigated using ATR-FTIR. Figures 1a and S2b show the FTIR spectra of the polyester films using different concentrations of allylated gallic acid and different reaction times. The presence of the absorption peaks at 1724 (C═O) and 1215 (C−C−O) cm^{-1} confirmed the formation of the polyester film when 1 wt % AG reacted with 0.1 wt % TMC for 20 min (Figure 1a; blue).[36] By decreasing the concentration of allylated gallic acid to 0.5% and maintaining the reaction time at 20 min, the absorption peaks that are characteristic of the ester groups became less visible. In contrast, the peak were more pronounced when the reaction time prolonged to 90 and 180 min (Figure S2b). At the same time, the intensity of the absorption bands characteristic of the PAN support (1454 (C−H) and 2243 (C≡N) cm^{-1})[37] decreased, indicating the formation of a thicker layer at a longer reaction time. A broad band in the range of 3200−3500 cm^{-1} was detected and attributed to residual hydroxyl groups, which are expected to enhance the membrane hydrophilicity. Thus, the reaction conditions strongly influence the polyester film formation because of lower reactivity of the phenolic OH groups compared with the conventional monomers involved in classical interfacial polymerization such as MPD.[38]

In addition, Figure 1a (red) shows the FTIR spectrum of the synthesized polyesteramide film, prepared using 1 wt % AG and 0.1 wt % MPD as polar-phase reactants. The spectrum revealed three unique peaks characteristic of the polyamide film at 1663, 1612, and 1541 cm^{-1} according to Tang et al.[39,40] The peaks were, respectively, assigned to the amide I band (C═O stretching, C−N stretching, and C−N deformation vibration in a secondary amide group), aromatic amide (N−H deformation vibration or C═C ring stretching vibration), and amide II band (N−H in plane bending and N−C stretching vibration of a −CO−NH group). The intensities of the absorption peaks that are characteristic of the ester group are lower for the polyesteramide compared with the polyester. An additional peak at around 3300 cm^{-1} was also observed on the spectra for the polyesteramide and polyamide control (TFC-$MPD_{0.1}$), which can be due to the overlapping of stretching vibrations for residual N−H and carboxylic groups.[40]

The olefin group produced a less pronounced peak at 1650 cm^{-1}, as observed on the spectrum for the phenolic monomer AG (Figure S2a). However, after polymerization, the peak at 1650 cm^{-1} remained noticeable, indicating that it will be

https://doi.org/10.1021/acssuschemeng.2c02637
ACS Sustainable Chem. Eng. XXXX, XXX, XXX−XXX

Table 2. Theoretical Elemental Compositions and Their Ratios Compared to Experimental Values Obtained for Different Samples

		elemental composition (%)						
sample		C	O	N	Cl	C/O	C/N	O/N
allyl gallate	experimental	69.4	27.9			2.5		
PAN	experimental	77.6	0.9	21.5		86.2	3.6	0
polyamide (TFC-$MPD_{0.1}$)	calculated (a)	71.4	14.3	14.3		5.0	5.0	1.0
	calculated (b)	71.4	19.0	9.5		3.8	7.5	2.0
	experimental	77.0	13.0	9.3	0.4	5.9	8.3	1.4
polyester (TFC-$AG_{1.0}$)	calculated (c,d)	67.9	32.1			2.1		
	experimental	71.5	26.4	1.2		2.7	59.6	22.0
polyesteramide (TFC-$AG_{1.0}$-$MPD_{0.1}$)	calculated (e)	69.4	22.2	8.3		3.1	8.3	2.7
	calculated (f)	69.4	25.0	5.6		2.8	12.5	4.5
	experimental	75.5	16.1	7.4	0.3	4.7	10.2	2.2

available for further functionalization (Figures 1a and S2b).[36] This is further validated by the solid-state NMR, where the peak characteristic of CH_2 was still observed at around 70 ppm for freestanding polyesteramide films (Figure S3).

The elemental composition and chemical binding information of the TFC membranes were obtained using survey and high-resolution XPS. The spectra of PAN and TFC membranes prepared using different ratios of polar-phase monomers, AG and MPD, are presented in Figures 1b−e and S4−S6. The formation of the polyester film was indicated by the increase in the oxygen content from 0.9% for the PAN support to 26.4% for TFC-$AG_{1.0}$, as shown in the survey spectra (Figure 1). However, the C/O ratio was greater than the estimated value based on the basic reaction patterns shown in Figure 2 and Table 2, which can be an indication of unreacted TMC moieties, suggesting a partial cross-linking degree of the film. To further understand the layer structure, the high-resolution XPS spectra of the C 1s and O 1s core levels for the AG monomer (Figure S4b,c) and TFC-$AG_{1.0}$ (Figure S6e,f) were evaluated. The C 1s core-level spectra were fitted using four components located at 284.5, 285.9, 288.5, and 291.1 eV, attributed to C═C/C−C, C−O, O−C═O, and $\pi-\pi^*$ shake-up satellites, respectively. The O 1s core-level spectra were fitted using two components at 531.1 and 532.4 eV corresponding to C═O and C−O. The increase of the initesity of the C═O bond (O 1s spectrum) and the counter decrease of the C−O bond intensity (C 1s spectrum) for the TFC-$AG_{1.0}$ confirmed the formation of the polyester layer. The relatively high intensity of the C−O band (O 1s spectrum) can be correlated with the unreacted OH and COOH groups from the AG and TMC, respectively.

The synthesis of the hybrid polyesteramide film involves polar-phase monomers with different reaction rates. The reaction of acyl halides with primary amines is a few orders of magnitude higher than that with hydroxyl groups.[38] Therefore, XPS was used to validate the formation of the polyesteramide film prepared using 1 wt % AG and 0.1 wt % MPD despite the difference in the reactivity of the monomers. Figure 1c−e shows the high-resolution XPS spectra of the C 1s, N 1s, and O 1s core levels. The presence of the binding energies that are characteristic of an ester (288.5 and 532.8 eV) and amide (287.7, 399.7 and 531.1 eV) groups demonstrate that the AG monomer reacts with the TMC and is not simply electrostatically adsorbed on the membrane during the reaction. Therefore, if we assume that AG and MPD can react to the same TMC unit, four basic reaction patterns can be identified, as shown in Figure 2. For comparison, the reaction between MPD and TMC has two basic patterns, fully crosslinked and fully linear.

An evaluation method similar to Tang et al.[39,40] was followed in this study to estimate the degree of cross-linking for the films. The measured atomic composition was compared with those expected for fully cross-linked and fully linear structures. We followed an analogous assumption, considering now the participation of the phenolic monomers, as shown in Figure 2. The C/O and O/N values for TFC-$AG_{1.0}$-$MPD_{0.1}$ were 4.7 and 2.2, respectively, which indicates a mixture of partially cross-linked and linear patterns. This shows a relative competition between the polar phase monomers to react with TMC. For the TFC-$MPD_{0.1}$, the theoretical O/N ratio ranges from 1.0 when all O and N atoms are associated with amide groups and 2.0 for linear polyamide with no cross-linking (Table 2). The measured value for TFC-$MPD_{0.1}$ revealed a different O/N ratio of 1.4, which indicates that the membranes were not fully cross-linked (77% C, 13% O, and 9.3% N, Figure 2 and Table 2). Residual N−H and carboxylic groups were also observed on the infrared spectrum and high-resolution spectra (Figures 1a and S6a−c). The XPS findings are in agreement with the FTIR data.

3.2. Membrane Morphology. The SEM images of the PAN support and TFC membranes are shown in Figures 3 and S7. The PAN support is highly porous with the pore size ranging from 20 to 40 nm, as shown in Figure S7a. Following the interfacial polymerization reaction, a dense polyesteramide film was formed on top of the support (Figure 3b,e). The results showed a different surface morphology compared to the conventional ridge and valley structure of the polyamide membranes (Figure 3c, f). This can be attributed to the fact that classical monomers containing primary amines have higher reaction rates with acyl halides than hydroxyl groups and display greater diffusivity into the organic phase as well, creating more convection pockets at the interface that translate into the ridge structure. Meanwhile, the phenolic monomer most likely experiences a lower diffusion rate into the opposite phase, and thus, a smoother polyester layer is observed in Figure 3a, d when 1 wt % AG was reacted with 0.1 wt % TMC for 20 min. By decreasing the concentration of AG to 0.5 wt % and varying the reaction time between 180−20 min, a thicker polyester film was observed (Figure S7b−d).

The surface topography of TFC membranes and free-standing films was further evaluated using AFM, and the results are summarized in Figures 3g−n, S8, and S9. The root mean square (R_{ms}) roughness of the TFC membrane prepared using 1 wt % AG and 0.1 wt % TMC at 20 min reaction time was 3.2

https://doi.org/10.1021/acssuschemeng.2c02637
ACS Sustainable Chem. Eng. XXXX, XXX, XXX−XXX

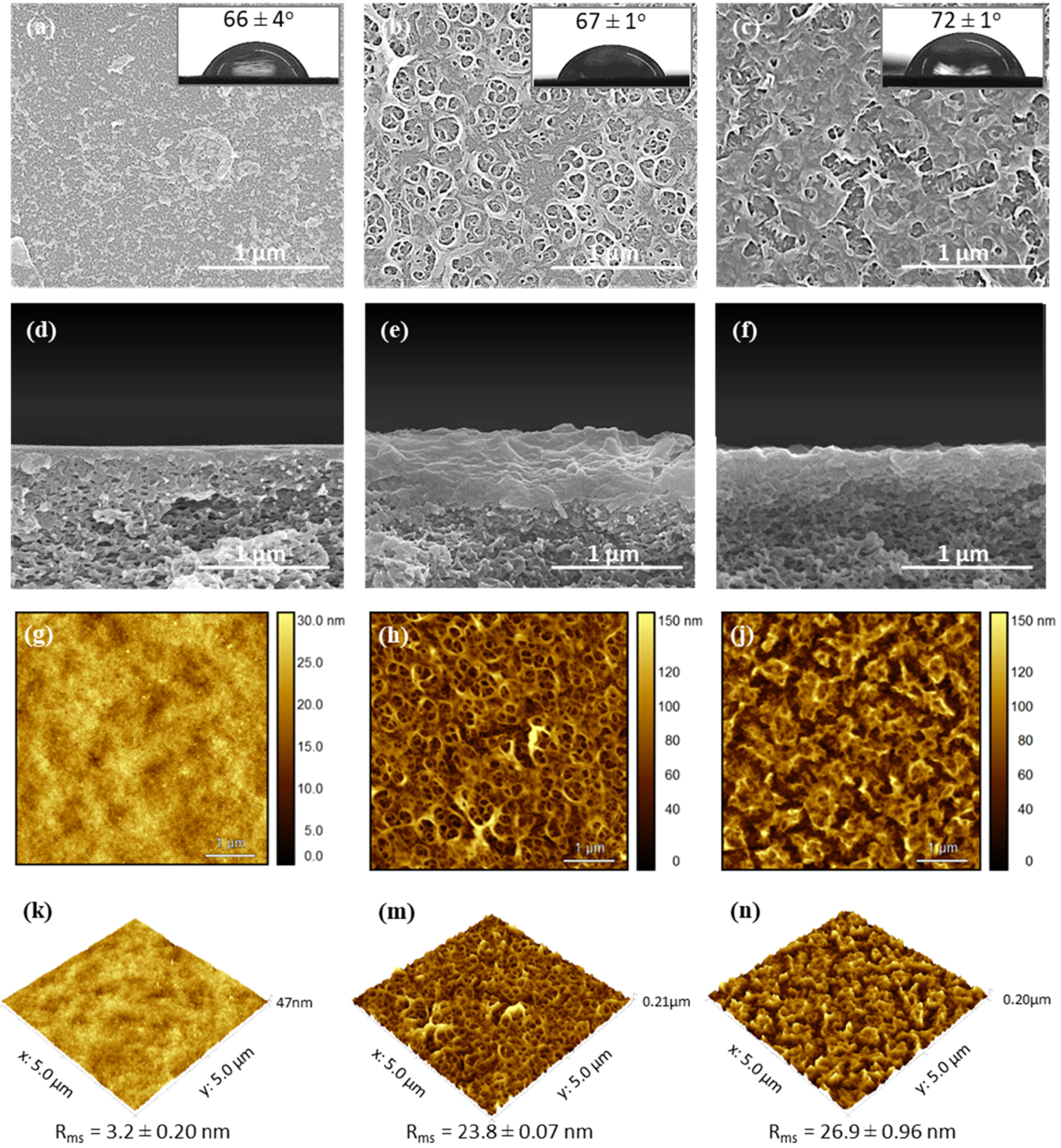

Figure 3. Morphologies of thin films. Surface (top) and cross-section (bottom) SEM images and contact angle measurements (inset) of (a, d) TFC-$AG_{1.0}$-t_{20}, (b, e) TFC-$AG_{1.0}$-$MPD_{0.1}$-t_{20}, and (c, f) TFC-$MPD_{0.1}$-t_{20}. AFM images (2D and 3D representation) of (g, k) TFC-$AG_{1.0}$-t_{20}, (h, m) TFC-$AG_{1.0}$-$MPD_{0.1}$-t_{20}, (j, n) TFC-$MPD_{0.1}$-t_{20}.

± 0.2 nm (Figure 3g, k), which was slightly greater than the value for the PAN support (2.8 ± 0.01 nm), as shown in Figure S8b and in line with the SEM images (Figure 3a, d). The addition of the phenolic monomer into the polar phase of the interfacial polymerization reaction slightly decreased the R_{ms} roughness from 26.9 ± 0.96 to 23.8 ± 0.07 nm for, respectively, polyamide and polyesteramide films (Figure 3m, n). The thickness of TFC membranes was further estimated based on the height profile of the corresponding freestanding films collected from the interface on a silicon wafer (Figure S9 and Table 3). We can observe that by varying the reaction time between 180−20 min, the film thickness decreased from 627 ± 109 to 103 ± 7 nm when 0.5 wt % AG was allowed to react with 0.1 wt % TMC. By increasing the concentration of AG to 1 wt % and maintaining the reaction time at 20 min, the thickness increased accordingly to 140 ± 24 nm. Further introduction of MPD to the polar phase slightly increased the mean thickness to 142 ± 23 nm.

https://doi.org/10.1021/acssuschemeng.2c02637
ACS Sustainable Chem. Eng. XXXX, XXX, XXX−XXX

Table 3. Thickness Profile of Freestanding Films Prepared at Different Reaction Times and Polar Phase Monomer Concentrations

sample	thickness [nm]
FS-$AG_{0.5}$-$TMC_{0.1}$-t_{180}	627 ± 109
FS-$AG_{0.5}$-$TMC_{0.1}$-t_{90}	454 ± 65
FS-$AG_{0.5}$-$TMC_{0.1}$-t_{20}	103 ± 7
FS-$AG_{1.0}$-$TMC_{0.1}$-t_{20}	140 ± 24
FS-$AG_{1.0}$-$MPD_{0.1}$-$TMC_{0.1}$-t_2	142 ± 23
FS-$MPD_{0.1}$-$TMC_{0.1}$-t_{20}	129 ± 21

The water contact angle of the polyester film was found to be 66 ± 4°, which is relatively hydrophilic compared to pure polyamide membranes (72 ± 1°), as shown in Figure 3a,c (insert). Furthermore, the surface ζ potential was recorded at pH 7 for TFC membranes prepared with different ratios of polar-phase monomers, AG and MPD. The surface ζ potential values are in the range of −71 ± 5 to −51 ± 2, indicating that all TFC membranes are negatively charged. The hydrophilicity and negative charge of the membranes can be attributed to unreacted OH and COOH groups of AG and TMC, as indicated by the FTIR and XPS spectra (Figure 1).

3.3. Nanofiltration Performance. The fabricated TFC membranes were tested for nanofiltration at room temperature to study the permeance of pure water and the separation performance of dye solutions (Figure 4). The permeance of pure water through the composite membranes prepared with the AG concentration of 0.5 wt % decreased from 53 ± 2 to 1.3 ± 0.2 L m^{-2} h^{-1} bar^{-1} with, respectively, an increase in the reaction time from 20 to 180 min, as shown in Figure 4a. A sharp decrease was observed by varying the reaction time from 20 to 60 min. This indicates an increase in the film thickness as the reaction time is increased, which correlates with thickness profiles estimated by AFM (Figure S9 and Table 3), and implied from the SEM images (Figure S7) and indirectly from the FTIR spectra (Figure S2b). This decrease in the permeance was coupled with an increase in the membrane selectivity for dyes of different molecular weights, which can suggest that defects or pinholes are also being mended with prolonged reaction times because of the low reactivity of the phenolic monomer with TMC (Figure 4c). Polyester composite membranes prepared from 0.5% AG with a reaction time greater than 90 min showed high rejection (>90%) for dyes with molecular weights over 697 g mol^{-1}. However, increasing the concentration of AG to 1 wt % and maintaining the reaction time at 20 min yielded a similar rejection curve with a pure water permeance of 47.6 ± 0.5 L m^{-2} h^{-1} bar^{-1} (Figure 4b, c). This indicates that the selectivity of the polyester film can be tuned for solute molecules smaller than 697 g mol^{-1} by varying the reaction time. Therefore, we further investigated the separation performance of methyl orange, 327 g mol^{-1}. The rejection of this solute increased from 29 to 91% for 20−180 min reaction, which demonstrates the formation of a tighter and thicker layer. The introduction of 0.1 wt % MPD to the polar phase, containing 1 wt % AG, retained this high rejection at only 20 min of reaction with 81% retention of methyl orange. By further increasing the concentration of MPD to 0.3 wt %, the rejection of methyl orange also improved to 98% (Figure 4b). This validates the higher reactivity of amino-functionalized monomers with TMC, which promotes a greater cross-linking of the network. We can also observe that the rejection of methyl orange directly correlates with the negative surface charge of the TFC membranes. Strongly charged polyamide membranes reported the highest rejection (Figure 4b, c). Therefore, the Donnan effect on the transport is expected to play an important role on the separation performance, considering that the investigated dyes are negatively charged (Table S1). The rejection of the dyes with specific molecular weights as shown in Figure 4c,

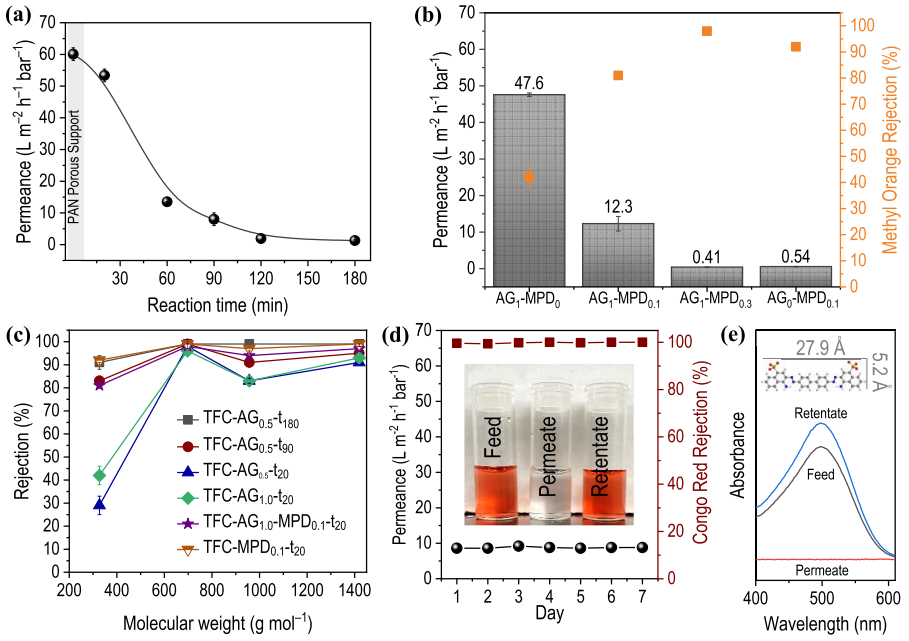

Figure 4. Nanofiltration performance. Pure water permeance through membranes prepared at (a) different reaction times 0−180 min at an AG concentration of 0.5 wt %. (b) Effect of MPD introduction to the polar phase of the reaction on the water permeance and methyl orange rejection. (c) Rejection of dyes by TFC membranes prepared using different reaction times and polar phase monomers ratio. (d) Long-term stability of TFC-$AG_{1.0}$-$MPD_{0.1}$ evaluated using 20 ppm Congo red aqueous solution. (e) UV absorption spectra of Congo red solution before and after permeation.

https://doi.org/10.1021/acssuschemeng.2c02637
ACS Sustainable Chem. Eng. XXXX, XXX, XXX−XXX

however, can indicate that the separation might be a combination of size exclusion and the Donnan effect.

TFC membranes prepared using different ratios of polar-phase monomers, AG and MPD, displays a permselectiviy tradeoff with the retention of methyl orange (Figure 4b). The permeance values increased from 0.5 ± 0.1 L m^{-2} h^{-1} bar^{-1} for the polyamide composite membranes to 12 ± 2 L m^{-2} h^{-1} bar^{-1} for the hybrid film and 47.6 ± 0.5 L m^{-2} h^{-1} bar^{-1} when pure AG was used as the polar-phase monomer. When the ratio of AG/MPD was decreased, the pure water permeance also decreased to 0.41 ± 0.02 L m^{-2} h^{-1} bar^{-1}. This demonstrates the significant contribution of AG integration into the synthesis of TFC membranes. The improved membrane performance can be correlated with the increasing hydrophilicity (Figure 3a–c) because not all the hydroxyl groups are involved in the layer formation (Figures 1a and S2b). Moreover, the thinner and loose structure obtained using only pure AG monomer enhanced the performance (Figure 3 and Table 3). In addition to the high permeance and rejection, the long-term stability of the polyesteramide composite membranes was confirmed by testing permeance and rejection of 20 Congo red solution for seven days. No significant changes in the permeance or the rejection were observed, as shown in Figure 4d, e.

A lower rejection and molecular weight cutoff are estimated by the filtration of PEGs with different molecular weights between 0.6 and 35 kg mol^{-1}, as shown in Figure S10. Unlike dyes, PEGs are highly hydrophilic molecules that might be able to penetrate through the film. The higher retention of dyes can be attributed to both size exclusion and electrostatic interactions because the membranes are negatively charged at neutral pH.

The rejection data of the inorganic salts by the polyesteramide composite membrane are shown in Figure S11. The inorganic salts rejection was lower than that of the dyes and followed the order Na_2SO_4 > $MgSO_4$ ≈ NaCl. The separation mechanism can be explained in terms of sieving and dielectric exclusion. The hydrated radius of the ions decreases in the following order: Mg^{+2}(4.28 Å) > SO_4^{-2} (3.79 Å) > Na^+(3.58 Å) > Cl^-(3.32 Å).[41] For negatively charged nanofiltration membranes, the solutes with higher anionic charge or lower cationic charge are rejected more efficiently.[18,31] Therefore, the rejection of Na_2SO_4 is sufficiently greater than $MgSO_4$ and NaCl. The performance of the composite membrane synthesized here, the high selectivity for dyes, and moderate inorganic salts permeation, is comparable to previously reported TFC membranes summarized in Table S2. This indicate that the naturally extracted allyated gallic acid has a potential for the production of TFC membranes for textile wastewater purification.

4. CONCLUSIONS

A naturally derived building block, allylated gallic acid, has been explored for the formation of thin-film composite membranes via interfacial polymerization reaction with trimesoyl chloride. The multifunctional phenolic monomer increased the hydrophilicity of the membrane compared to analogous ones prepared with the conventional monomer MPD because of a small part of nonreacted hydroxyl groups remaining. The hydrophilic nature of phenols, the morphology, and the loose structure of the polyester layer exhibited a water permeance of 47.6 ± 0.5 L m^{-2} h^{-1} bar^{-1}. The AG reactivity with acyl chloride is lower than that of commonly used monomers, such as MPD. The introduction of a co-monomer in the aqueous phase improved the formation of the films and resulted in better separation performance. The chemical composition and availability of the unreacted olefin group were confirmed via FTIR, which is of great benefit for tuning the surface properties through the activation of the terminal group and covalent binding to the surface. A possible approach is the use of thiol-ene induced reaction to graft polymer brushes onto the surface to enhance the antifouling resistance. Such conjugation can be used for a variety of other functionalization to enable applications beyond membrane separation such as catalyst immobilization and biosensors.

AUTHORS CONTRIBUTION

S.N. conceived the project and supervised. B.A. designed the experiments, performed the material synthesis, carried out the material characterization and nanofiltration performance evaluation. F.A. contributed to part of the characterization. G.S. co-supervised. B.A. and P.M. analyzed the spectroscopic data. B.A. and S.N. wrote the first draft of the manuscript. All authors discussed findings and assisted in comprehending the results.

ASSOCIATED CONTENT

Supporting Information

The Supporting Information is available free of charge at https://pubs.acs.org/doi/10.1021/acssuschemeng.2c02637.

Chemical structures of selected natural phenols; FTIR, solid NMR, and XPS characterization of monomers and membranes; SEM and AFM images of membranes; gel chromatography of the PEG mixture and trimethylol propane ethoxylate solutions in water as feed and permeate for the membrane performance test; chemical structures and characteristics of testing dyes; and performances compared with previous reports in the literature (PDF)

AUTHOR INFORMATION

Corresponding Author

Suzana P. Nunes − *Environmental Science and Technology, Biological and Environmental Science and Engineering Division, Advanced Membrane and Porous Material Center, and Chemical Science, Physical Science and Engineering Division, King Abdullah University of Science and Technology (KAUST), 23955-6900 Thuwal, Saudi Arabia; Chemical Engineering, Physical Science and Engineering Division, King Abdullah University of Science and Technology (KAUST), 23955-6900 Thuwal, Saudi Arabia;* orcid.org/0000-0002-3669-138X; Email: Suzana.nunes@kaust.edu.sa

Authors

Banan Alhazmi − *Environmental Science and Technology, Biological and Environmental Science and Engineering Division and Advanced Membrane and Porous Material Center, King Abdullah University of Science and Technology (KAUST), 23955-6900 Thuwal, Saudi Arabia*

Fadhilah Alduraiei − *Environmental Science and Technology, Biological and Environmental Science and Engineering Division and Advanced Membrane and Porous Material Center, King Abdullah University of Science and Technology (KAUST), 23955-6900 Thuwal, Saudi Arabia*

https://doi.org/10.1021/acssuschemeng.2c02637
ACS Sustainable Chem. Eng. XXXX, XXX, XXX−XXX

Priyanka Manchanda − *Environmental Science and Technology, Biological and Environmental Science and Engineering Division and Advanced Membrane and Porous Material Center, King Abdullah University of Science and Technology (KAUST), 23955-6900 Thuwal, Saudi Arabia*

Stefan Chisca − *Environmental Science and Technology, Biological and Environmental Science and Engineering Division and Advanced Membrane and Porous Material Center, King Abdullah University of Science and Technology (KAUST), 23955-6900 Thuwal, Saudi Arabia*

Gyorgy Szekely − *Advanced Membrane and Porous Material Center and Chemical Science, Physical Science and Engineering Division, King Abdullah University of Science and Technology (KAUST), 23955-6900 Thuwal, Saudi Arabia;* orcid.org/0000-0001-9658-2452

Complete contact information is available at: https://pubs.acs.org/10.1021/acssuschemeng.2c02637

Notes

The authors declare no competing financial interest.

■ ACKNOWLEDGMENTS

This research was supported by the King Abdullah University of Science and Technology (KAUST). We specially thank Nimer Wehbe for running the XPS experiments, Abdul-hamid Emwas for the ssNMR data, and Long Chen for carrying out the AFM experiments.

■ REFERENCES

(1) Rys, P.; Zollinger, H. *Fundamentals of the Chemistry and Application of Dyes*; Wiley-Interscience, 1972.

(2) Reife, A.; Freeman, H. S. *Environmental chemistry of dyes and pigments*; John Wiley & Sons, 1996.

(3) Jain, R.; Sikarwar, S. Photocatalytic and adsorption studies on the removal of dye Congo red from wastewater. *Int. J. Environ. Pollution* **2006**, *27*, 158−178.

(4) Liang, C.-Z.; Sun, S.-P.; Li, F.-Y.; Ong, Y.-K.; Chung, T.-S. Treatment of highly concentrated wastewater containing multiple synthetic dyes by a combined process of coagulation/flocculation and nanofiltration. *J. Membr. Sci.* **2014**, *469*, 306−315.

(5) Mulder, M. *Basic Principles of Membrane Technology*, 2nd ed.; Kluwer Academic, 1996.

(6) Nunes, S. P.; Peinemann, K. V. *Membrane Technology in the Chemical Industry*, 2nd Revised and Extended ed.; Wiley-VCH, 2006.

(7) Mohammad, A. W.; Teow, Y. H.; Ang, W. L.; Chung, Y. T.; Oatley-Radcliffe, D. L.; Hilal, N. Nanofiltration Membranes Review: Recent Advances and Future Prospects. *Desalination* **2015**, *356*, 226−254.

(8) Cadotte, J. E. Interfacially synthesized reverse osmosis membrane; 4,277,344, 1981.

(9) Cadotte, J. E.; Petersen, R. J.; Larson, R. E.; Erickson, E. E. A New Thin-film Composite Seawater Reverse Osmosis Membrane. *Desalination* **1980**, *32*, 25−31.

(10) Cadotte, J. E.; Petersen, R. J. Thin-Film Composite Reverse-Osmosis Membranes: Origin, Development, and Recent Advances. In *Synthetic Membranes*; ACS Symposium Series, Vol. *153*; American Chemical Society, 1981; Chapter 21Vol. 153 , pp. 305−326.

(11) Lu, X.; Elimelech, M. Fabrication of desalination membranes by interfacial polymerization: history, current efforts, and future directions. *Chem. Soc. Rev.* **2021**, *50*, 6290−6307.

(12) Seah, M. Q.; Lau, W. J.; Goh, P. S.; Tseng, H.-H.; Wahab, R. A.; Ismail, A. F. Progress of interfacial polymerization techniques for polyamide thin film (nano) composite membrane fabrication: a comprehensive review. *Polymer* **2020**, *12*, 2817.

(13) Zhang, F.; Fan, J. B.; Wang, S. Interfacial polymerization: from chemistry to functional materials. *Angew. Chem., Int. Ed.* **2020**, *59*, 21840−21856.

(14) Van der Bruggen, B.; Daems, B.; Wilms, D.; Vandecasteele, C. Mechanisms of retention and flux decline for the nanofiltration of dye baths from the textile industry. *Sep. Purif. Technol.* **2001**, *22-23*, 519−528.

(15) Yang, X.; Huang, J.; Yang, F.; Wang, W.; Xue, C.; Zhou, W.; Wu, Y.; Shao, L.; Zhang, Y. Metal-organophosphate biphasic interfacial coordination reaction synthesizing nanofiltration membranes with the ultrathin selective layer, excellent acid-resistance and antifouling performance. *J. Membr. Sci.* **2022**, *653*, 120521.

(16) Zhu, J.; Wang, J.; Uliana, A. A.; Tian, M.; Zhang, Y.; Zhang, Y.; Volodin, A.; Simoens, K.; Yuan, S.; Li, J.; Lin, J.; Bernaerts, K.; van der Bruggen, B. Mussel-Inspired Architecture of High-Flux Loose Nanofiltration Membrane Functionalized with Antibacterial Reduced Graphene Oxide−Copper Nanocomposites. *ACS Appl. Mater. Interface* **2017**, *9*, 28990−29001.

(17) Cheng, X. Q.; Wang, Z. X.; Zhang, Y.; Zhang, Y.; Ma, J.; Shao, L. Bio-inspired loose nanofiltration membranes with optimized separation performance for antibiotics removals. *J. Membr. Sci.* **2018**, *554*, 385−394.

(18) Veríssimo, S.; Peinemann, K. V.; Bordado, J. Influence of the diamine structure on the nanofiltration performance, surface morphology and surface charge of the composite polyamide membranes. *J. Membr. Sci.* **2006**, *279*, 266−275.

(19) Lee, H.; Dellatore, S. M.; Miller, W. M.; Messersmith, P. B. Mussel-Inspired Surface Chemistry for Multifunctional Coatings. *Science* **2007**, *318*, 426−430.

(20) Zhao, J.; Su, Y.; He, X.; Zhao, X.; Li, Y.; Zhang, R.; Jiang, Z. Dopamine Composite Nanofiltration Membranes Prepared by Self-polymerization and Interfacial Polymerization. *J. Membr. Sci.* **2014**, *465*, 41−48.

(21) Pérez-Manríquez, L.; Behzad, A. R.; Peinemann, K.-V. Sub-6 nm Thin Cross-Linked Dopamine Films with High Pressure Stability for Organic Solvent Nanofiltration. *Macromol. Mater. Eng.* **2016**, *301*, 1437−1442.

(22) Zhang, Y.; Cheng, X.; Jiang, X.; Urban, J. J.; Lau, C. H.; Liu, S.; Shao, L. Robust natural nanocomposites realizing unprecedented ultrafast precise molecular separations. *Mater. Today* **2020**, *36*, 40−47.

(23) Barrett, D. G.; Sileika, T. S.; Messersmith, P. B. Molecular Diversity in Phenolic and Polyphenolic Precursors of Tannin-inspired Nanocoatings. *Chem. Commun.* **2014**, *50*, 7265−7268.

(24) Sileika, T. S.; Barrett, D. G.; Zhang, R.; Lau, K. H. A.; Messersmith, P. B. Colorless Multifunctional Coatings Inspired by Polyphenols Found in Tea, Chocolate, and Wine. *Angew. Chem., Int. Ed.* **2013**, *52*, 10766−10770.

(25) Park, S.-H.; Alammar, A.; Fulop, Z.; Pulido, B. A.; Nunes, S. P.; Szekely, G. Hydrophobic thin film composite nanofiltration membranes derived solely from sustainable sources. *Green Chem.* **2021**, *23*, 1175−1184.

(26) Pérez-Manríquez, L.; Neelakanda, P.; Peinemann, K.-V. Morin-based Nanofiltration Membranes for Organic Solvent Separation Processes. *J. Membr. Sci.* **2018**, *554*, 1−5.

(27) Abdellah, M. H.; Pérez-Manríquez, L.; Puspasari, T.; Scholes, C. A.; Kentish, S. E.; Peinemann, K. V. Effective Interfacially Polymerized Polyester Solvent Resistant Nanofiltration Membrane from Bioderived Materials. *Adv. Sustain. Syst.* **2018**, *2*, 1800043.

(28) Abdellah, M. H.; Pérez-Manríquez, L.; Puspasari, T.; Scholes, C. A.; Kentish, S. E.; Peinemann, K.-V. A Catechin/Cellulose Composite Membrane for Organic Solvent Nanofiltration. *J. Membr. Sci.* **2018**, *567*, 139−145.

(29) Zhao, S.; Wang, Z. A loose nano-filtration membrane prepared by coating HPAN UF membrane with modified PEI for dye reuse and desalination. *J. Membr. Sci.* **2017**, *524*, 214−224.

(30) Liu, S.; Wang, Z.; Song, P. Free Radical Graft Copolymerization Strategy To Prepare Catechin-Modified Chitosan Loose Nanofiltration (NF) Membrane for Dye Desalination. *ACS Sustainable Chem. Eng.* **2018**, *6*, 4253−4263.

(31) Zhang, Y.; Su, Y.; Peng, J.; Zhao, X.; Liu, J.; Zhao, J.; Jiang, Z. Composite nanofiltration membranes prepared by interfacial polymerization with natural material tannic acid and trimesoyl chloride. *J. Membr. Sci.* **2013**, *429*, 235−242.
(32) Li, Q.; Liao, Z.; Fang, X.; Xie, J.; Ni, L.; Wang, D.; Qi, J.; Sun, X.; Wang, L.; Li, J. Tannic acid assisted interfacial polymerization based loose thin-film composite NF membrane for dye/salt separation. *Desalination* **2020**, *479*, 114343.
(33) Perez-Manriquez, L.; Neelakanda, P.; Peinemann, K. V. Tannin-based Thin-film Composite Membranes for Solvent Nanofiltration. *J. Membr. Sci.* **2017**, *541*, 137−142.
(34) Fei, F.; Le Phuong, H. A.; Blanford, C. F.; Szekely, G. Tailoring the performance of organic solvent nanofiltration membranes with biophenol coatings. *ACS Appl. Polym. Mater.* **2019**, *1*, 452−460.
(35) Sileika, T. S.; Barrett, D. G.; Zhang, R.; Lau, K. H. A.; Messersmith, P. B. Colorless multifunctional coatings inspired by polyphenols found in tea, chocolate, and wine. *Angew. Chem. Int. Ed.* **2013**, *125*, 10966−10970.
(36) Silverstein, R. M.; Webster, F. X.; Kiemle, D. J.; Bryce, D. L. *Spectrometric Identification of Organic Compounds* (in English) ; John Wiley & Sons, Ltd.: 2015.
(37) Karbownik, I.; Rac-Rumijowska, O.; Fiedot-Toboła, M.; Rybicki, T.; Teterycz, H. The Preparation and Characterization of Polyacrylonitrile-Polyaniline (PAN/PANI) Fibers. *Materials* **2019**, *12*, 664.
(38) Zhang, R.; Yu, S.; Shi, W.; Wang, W.; Wang, X.; Zhang, Z.; Li, L.; Zhang, B.; Bao, X. A novel polyesteramide thin film composite nanofiltration membrane prepared by interfacial polymerization of serinol and trimesoyl chloride (TMC) catalyzed by 4-dimethylaminopyridine (DMAP). *J. Membr. Sci.* **2017**, *542*, 68−80.
(39) Tang, C. Y.; Kwon, Y.-N.; Leckie, J. O. Probing the nano- and micro-scales of reverse osmosis membranes—A comprehensive characterization of physiochemical properties of uncoated and coated membranes by XPS, TEM, ATR-FTIR, and streaming potential measurements. *J. Membr. Sci.* **2007**, *287*, 146−156.
(40) Tang, C. Y.; Kwon, Y.-N.; Leckie, J. O. Effect of membrane chemistry and coating layer on physiochemical properties of thin film composite polyamide RO and NF membranes: I. FTIR and XPS characterization of polyamide and coating layer chemistry. *Desalination* **2009**, *242*, 149−167.
(41) Nightingale, E. R., Jr. Phenomenological theory of ion solvation, effective radii of hydrated ions. *J. Phys. Chem.* **1959**, *63*, 1381−1387.

https://doi.org/10.1021/acssuschemeng.2c02637
ACS Sustainable Chem. Eng. XXXX, XXX, XXX−XXX